



Centrifugal Pendulum Vibration Absorbers: An Experimental and Theoretical Investigation

ALAN G. HADDOW and STEVEN W. SHAW

Department of Mechanical Engineering, Michigan State University, East Lansing, MI 48824, U.S.A.

(Received: 19 June 2001; accepted: 21 July 2002)

Abstract. This paper presents results from tests completed on a rotor system fitted with pendulum-type centrifugal torsional vibration absorbers. A review of the associated theoretical background is also given and the experimental and theoretical results are compared and contrasted. An overview of the test apparatus is provided and its unique features are discussed. To the best knowledge of the authors, this is the first time that a systematic study of the dynamic behavior of torsional vibration absorbers has been undertaken in a controlled environment.

Keywords: Absorbers, CPVA, TVA, torsional.

1. Introduction

Centrifugal Pendulum Vibration Absorbers (CPVAs) are used to suppress torsional vibrations in rotating machinery. They are widely employed in light aircraft engines and helicopter rotors. They are also used in some high-performance automotive racing engines, diesel camshafts, and other places where torsional vibrations at a given order are troublesome. These absorbers consist essentially of pendulums suspended from a rotor such that they can oscillate in a plane perpendicular to the axis of rotation. By proper selection of the suspension point and effective pendulum length, the absorbers can be tuned to address torsional vibrations at a given order of rotation. A key characteristic of these absorbers is that they remain tuned at all rotation speeds.

In application, these absorber systems are composed of a set of identical pendulums that are stationed along and about the axis of rotation. Recent analytical work has shown that systems of identical absorbers are dynamically very rich and can exhibit a variety of dynamic instabilities that affect their operating range and effectiveness [1].

While pendulum absorbers have been in use for over half a century, they continue to find new applications due to increasingly stringent vibration requirements in a variety of fields. Previous research has focused mainly on analysis and simulations for systematic design studies, but experimental studies are very limited and have all been tailored to specific applications [2]. In contrast, the present experimental study is, to the authors' knowledge, the first systematic exploration of a design space for pendulum absorbers. Specifically, it is the first study in which one can adjust the relative tuning of the absorber to the applied torque, as well as the torque amplitude, 'on the fly'. This allows one to quickly determine the optimal absorber tuning for maximum effectiveness over a given torque range.

The paper is organized as follows: The next section provides a review of the associated theoretical background. Governing equations, their approximate solutions, and definitions of the various parameters are stated without detailed derivation, but relevant references are

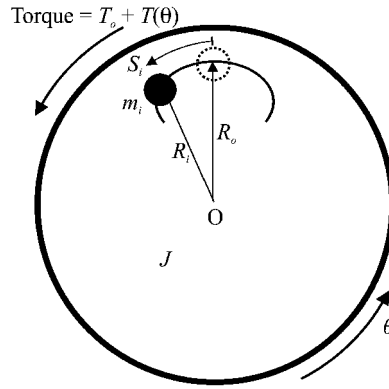


Figure 1. A schematic view of CPVAs mounted on a rotor of inertia J . For clarity, only the i^{th} absorber, of individual mass m_i , is shown. s_i is its displacement measured along the arc length of the path.

cited. The various steady-state solutions that are possible and their stability are also discussed. An overview of the experimental facility and its capabilities are described, and experimental results are presented and compared to the theoretical predictions. The paper closes with some concluding remarks and discusses the direction of future work.

2. Theoretical Background

This section outlines the analysis that provides the theoretical predictions used in the comparisons with experimental data. Only a summary is provided; the full development can be found in [1].

2.1. EQUATIONS OF MOTION

The simplest model that captures the essential dynamics of interest consists of a rigid rotor to which are fitted several point mass absorbers that move along prescribed paths relative to the rotor. The rotor is subjected to an applied torque that fluctuates at a given order of rotation, n , and the absorber paths are selected such that their motion counteracts the applied torque.

We consider a system of N CPVAs mounted on a rotor of inertia J (Figure 1). The equations of motion for the absorbers and the rotor are derived using Lagrange’s method for general absorber paths. It is convenient to recast these equations using the rotor angle θ as the independent variable, replacing time. This renders the excitation in a more standard form in which it is periodic in the independent variable. This change of variable, nondimensionalization of the system parameters and dynamic variables, and the assumption that all absorber masses and paths are identical, results in the following equations of motion [1]

$$vs_i'' + [s_i' + \tilde{g}(s_i)]v' - \frac{1}{2} \frac{dx(s_i)}{ds} v = -\mu_a s_i', \quad i = 1, \dots, N, \tag{1}$$

$$\begin{aligned} & \frac{\varepsilon}{N} \sum_{i=1}^N \left[\frac{dx(s_i)}{ds} s_i' v^2 + x(s_i) v v' + \tilde{g}(s_i) s_i' v v' + \tilde{g}(s_i) s_i'' v^2 + \frac{d\tilde{g}(s_i)}{ds} s_i^2 v^2 \right] + v v' \\ & = \frac{\varepsilon}{N} \mu_a \sum_{i=1}^N \tilde{g}(s_i) s_i' v - \mu_o v + \Gamma_o + \Gamma(\theta), \end{aligned} \tag{2}$$

where terms are defined as follows: The generalized coordinates for the $N + 1$ degrees of freedom are: s_i represents the displacement of the i^{th} absorber, as measured along the arc length of the path and normalized by R_o (defined below), and v is the nondimensional measure of the rotor angular velocity, normalized by the average rotor angular velocity Ω . Primes denote differentiation with respect to θ . The absorber path is described in the functions $x(s)$, which represents the square of the distance from the center of rotation to the absorber at its location s , and

$$\tilde{g}(s) = \sqrt{x(s) - \frac{1}{4} \left(\frac{dx(s)}{ds} \right)^2},$$

which is related to the tangent of the path. The nondimensional damping coefficients for the absorbers and rotor are denoted by μ_a , and μ_o , respectively. The parameter ε represents the ratio of the effective rotational inertia of all absorbers to J . For a point mass $\varepsilon = (mR_o^2)/J$ where m is the total absorber mass and R_o is the distance from the center of rotation to the absorber when it is at its vertex, corresponding to $s = 0$. The torque is composed of two terms, a constant, Γ_o , and a fluctuating component, $\Gamma(\theta)$. These torques have been normalized by the kinetic energy of the rotor, $J\Omega^2$. The fluctuating torque generally contains several harmonics, but typically only one or two harmonics have significant amplitude, and therefore we approximate the fluctuating torque by its dominant harmonic, taken to be of order n , as follows: $\Gamma(\theta) = \Gamma_\theta \sin(n\theta)$. For example, in single cylinder four-stroke internal combustion engines, n is equal to one-half.

2.2. THE ABSORBER PATH

The system equations can be formulated in terms of a general path with two design parameters, which can be selected in order to achieve certain goals in terms of absorber performance. In the present experimental study only circular paths are considered, since they are the simplest to manufacture, and they are in wide use in practice. This reduces the problem to a single path design parameter, related to the absorber tuning.

Denman [3] offers a formulation for the path parameters such that they correspond to small and large amplitude characteristics, respectively. The linear tuning of the path is given by a parameter \tilde{n} , which fixes the small amplitude (linearized) natural frequency of the absorbers to be $\tilde{n}\Omega$, when the rotor spins at a constant rate Ω . It is a central feature of these absorbers that this tuning frequency is proportional to the mean rotation rate, Ω , since this allows the absorber to remain tuned to a given order, \tilde{n} , at all rotation speeds. Based on purely linear considerations, the order of the path for a CPVA should be tuned to the frequency of the disturbance torque, that is, $\tilde{n} = n$. In the linear, undamped case this makes the absorber perfectly effective, since the rotor vibrations are completely eliminated. However, moderate to large absorber motions dictate that nonlinear effects be accounted for [4]. These arise from the frequency-amplitude dependence of the absorber and cause the absorber to become detuned at moderate amplitudes. This can lead to instabilities with devastating consequences [4]. The typical approach to avoiding these catastrophes is to incorporate a small level of intentional linear mistuning on the path, such that $\tilde{n} > n$. This allows the absorber to come into better tuning at moderate amplitudes; this is a technique implemented in practice [4].

In the equations of motion an expression for $x(s)$ is needed. The following expression can be reached by expanding in s ,

$$x(s) = 1 - \tilde{n}^2 s^2 + \gamma s^4 + O(s^6), \quad (3)$$

where, for circular paths,

$$\gamma = \frac{1}{12} \tilde{n}^2 (\tilde{n}^2 + 1)^2$$

(see [3]). The function $x(s)$ can be thought of as a type of potential function, where the quadratic term dictates the linear system behavior (frequency) and the quartic term determines the nonlinear behavior (the frequency-amplitude dependence). With these positive values of γ , the nonlinearity is softening, as expected.

A dynamic analysis for a compound centrifugal pendulum of the type considered in the present experiments yields the following result for the absorber tuning

$$\tilde{n} = \sqrt{rR/(r^2 + \rho^2)}, \quad (4)$$

where R is the distance from the center of rotation to the pendulum pivot point, r is the effective pendulum length (the distance from the pivot to the center of mass), and ρ is the radius of gyration of the pendulum about its center of mass. For a pendulum with a point mass ($\rho = 0$) this simplifies to the well-known result, $\tilde{n} = \sqrt{R/r}$, where $R_0 = R + r$ in terms of the point mass notation (Figure 1).

2.3. SCALING AND ASYMPTOTIC ANALYSIS

The equations of motion are analyzed by employing a scaling of parameters and dynamic variables that is based on the physical nature of the system. The underlying small parameter is the inertia ratio, ε , that in practice is typically on the order of 10^{-3} to 10^{-1} . Also, the nondimensional torque variables are scaled by the kinetic energy of the rotor, and are therefore also small. In addition, since the absorbers remain tuned at all rotor speeds, they are designed to have small damping. Therefore, the parameters associated with these quantities will also be scaled by ε .

When these small variables are all zero, the undamped, unforced rotor simply spins at constant rate and the absorbers sit at their respective vertices. Thus, the perturbation is carried out about the operating condition $(s_i, v) = (0, 1)$. The scaling allows one to capture the leading order effects of nonlinearity, damping, and the applied torque near this operating point. The required scaling orders for the parameters and dynamic variables are derived in [1], and are found to be

$$\mu_a = \varepsilon \tilde{\mu}_a, \quad \mu_o = \varepsilon \tilde{\mu}_o, \quad \Gamma_o = \varepsilon \tilde{\Gamma}_o, \quad \Gamma(\theta) = \varepsilon^{3/2} \tilde{\Gamma}(\theta),$$

$$\tilde{n} = n(1 + \varepsilon\sigma), \quad s_i = \varepsilon^{1/2} z_i, \quad v = 1 + \varepsilon^{3/2} w,$$

where σ represents a measure of the mistuning of the absorber paths, and the other scaled variables are defined in an obvious manner. Note that w represents deviations in the rotor speed from the desired (constant) value. The path functions x and \tilde{g} are also scaled in ε , on account of the above scaling of s_i and \tilde{n} .

These scaled parameters and variables are substituted into the equations of motion, which are then expanded in terms of ε . Dealing first with the rotor equation, Equation (2), and equating the coefficients of ε^1 , one obtains $\tilde{\Gamma}_o = \tilde{\mu}_o$. This is simply a balance of the mean rotor torque with the mean bearing resistance torque (which is given by $\tilde{\mu}_o$ since the average

rotor speed is unity). Returning to Equation (2) and equating the coefficients of $\varepsilon^{3/2}$, one can show that

$$w' = \tilde{\Gamma}(\theta) - \frac{1}{N} \sum_{j=1}^N z_j''.$$

This equation can be used to uncouple the equations of motion, as described subsequently. However, it is also useful for determining the torsional vibrations of the rotor, which correspond to fluctuations about the average rotor speed. This is conveniently measured by the angular acceleration of the rotor, which is given by $vv' = \varepsilon^{3/2}w' + \text{HOT}$ (this is $\dot{\theta}/\Omega^2$ expressed in terms the independent variable θ). Hence, when the fluctuating component of the applied torque is taken to be harmonic of order n , the rotor acceleration is given by

$$\varepsilon^{3/2}w' = \varepsilon^{3/2} \left\{ \frac{-1}{N} \sum_{j=1}^N z_j'' + \tilde{\Gamma}_\theta \sin(n\theta) \right\} + \text{HOT}. \quad (5)$$

This is a linear result that describes the effects of the applied torque and the motions of the absorbers on the rotor. The nonlinear character of the system response is accounted for through the absorbers' motion, z_i .

To study this motion, the same procedure is employed as before, but the scaled parameters are now substituted into Equation (1), to yield

$$\varepsilon^{1/2}\{z_i'' + n^2 z_i + \varepsilon[-2\gamma z_i^3 + 2n^2 \sigma z_i + \tilde{\mu}_a z_i' + w']\} + \text{HOT} = 0, \quad (6)$$

where $i = 1, \dots, N$. The previous expression for w' , Equation (5), can be substituted into these equations, thereby eliminating the rotor dynamics from the absorber equations. A convenient form of the absorber equations is obtained by using their leading order term to replace z_j'' by $-n^2 z_j$ in Equation (5), resulting in

$$z_i'' + n^2 z_i = \varepsilon \left[2\gamma z_i^3 - 2n^2 \sigma z_i - \tilde{\mu}_a z_i' - \frac{n^2}{N} \sum_{j=1}^N z_j - \tilde{\Gamma}_\theta \sin(n\theta) \right] + \text{HOT}, \quad i = 1, \dots, N, \quad (7)$$

where it may be recalled that $\tilde{n} = n(1 + \varepsilon\sigma)$ defines the absorber mistuning parameter σ .

Some comments on these equations are in order. First, the effects of the rotor dynamics on the absorbers are captured in terms of the applied torque and the torques from all absorbers acting on the rotor, which are contained in the summation term. Also, the only nonlinear effect that appears at this order is the one due to the path, i.e., $2\gamma z_i^3$. Missing at this order are all of the nonlinear terms that arise from the kinematic coupling of the rotation and the absorber motion. In addition, these equations are weakly nonlinear, due to the amplitude scaling, and weakly coupled, due to the small inertia ratio. The system of absorbers has some very special dynamical features, including the facts that each absorber has an identical unperturbed natural frequency, and each absorber is resonantly excited by the fluctuating applied torque. Furthermore, the absorbers are all coupled to one another in exactly the same manner. When the absorbers are identical, the system possesses symmetry properties that can be used to analyze the system dynamics [5, 6]. Here, however, the method of averaging is used to determine

approximate solutions of these equations. The usual transformation to amplitude and phase coordinates is used,

$$\left. \begin{aligned} z_i &= a_i \sin(n\theta + \phi_i) \\ z'_i &= na_i \cos(n\theta + \phi_i) \end{aligned} \right\}. \quad (8)$$

This results in the following equations, which are suitable for averaging,

$$\begin{aligned} a'_i &= \frac{\varepsilon}{n} f_i \cos(n\theta + \phi_i) + \text{HOT}, \\ \phi'_i &= -\frac{\varepsilon}{na_i} f_i \sin(n\theta + \phi_i) + \text{HOT}, \end{aligned} \quad (9)$$

where

$$\begin{aligned} f_i &= 2\gamma a_i^3 \sin^3(n\theta + \phi_i) - 2n^2 \sigma a_i \sin(n\theta + \phi_i) \\ &\quad - \tilde{\mu}_a na_i \cos(n\theta + \phi_i) - \frac{n^2}{N} \sum_{j=1}^N a_j \sin(n\theta + \phi_j) \\ &\quad - \tilde{\Gamma}_\theta \sin(n\theta). \end{aligned} \quad (10)$$

These equations are averaged over one period, $2\pi/n$, leading to a set of autonomous equations in terms of (a_i, ϕ_i) . The averaged equations have been used to investigate the existence and stability of many types of motion [1].

2.4. THE SYNCHRONOUS RESPONSE

The case of interest here is the synchronous response, where all absorbers move with identical amplitude and phase. This is the response that is assumed when one sizes the absorber inertia in practice. Assuming that the absorber amplitudes are given by $a_i = r_z, i = 1, \dots, N$ and the phases are likewise equal, it is determined that the steady state response amplitude is related to the system and the torque parameters by

$$\tilde{\Gamma}_\theta = 2n \sqrt{\left[\frac{\tilde{\mu}_a}{2} r_z \right]^2 + \left[\frac{3\gamma}{4n} r_z^3 - n \left(\sigma + \frac{1}{2} \right) r_z \right]^2}. \quad (11)$$

This is the same result one would obtain if all absorbers were a single, equivalent mass. However, the stability problem is more complicated, due to the presence of multiple absorbers.

In applications, the order of the applied torque, n , is given, and the general design problem is to find a mistuning, σ , such that the rotor vibrations, as measured by the rotor acceleration, are small over a wide range of torque levels. Once the mistuning is set by hardware design, the operational features of the absorber are fixed and can be described by the rotor response as a function of torque level. Figure 2 shows a typical response curve for rotor acceleration versus the amplitude of the fluctuating torque for a fixed value of mistuning. Note that the system has a classical hysteresis behavior with two saddle-node, or jump, bifurcations, denoted here as 'J' points. In addition, at a lower torque another bifurcation occurs, at point 'N', in which the synchronous response continues to exist, but becomes unstable. Point 'N' occurs at the point of horizontal tangency [1]. That is, stability of the synchronous response can be lost in two very distinct ways. The ones associated with points 'J' in Figure 2 are identical to the equivalent

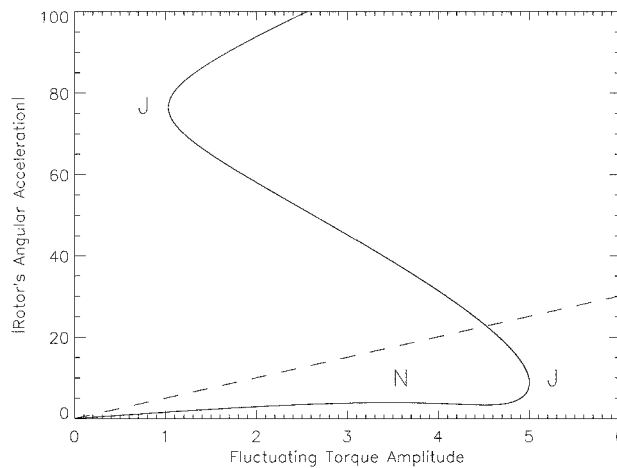


Figure 2. Angular acceleration versus alternating torque level for a fixed $n < \tilde{n}$. The dashed line represents the solution with the absorbers locked in position.

single mass case, since the full symmetry of the synchronous response is preserved. However, the second type of instability, associated with point 'N', occurs at a torque amplitude lower than the upward jump point. This instability leads to multiple solution branches emanating from the synchronous solution, and is inherently related to the symmetry of the system. There are many such branches and the resulting dynamics is quite complicated, due to the fact that a multiplicity of eigenvalues become simultaneously unstable at the bifurcation point. The branches involve responses with lower levels of symmetry, in which various subgroups of absorbers undergo mutually synchronous responses. This bifurcation is typically observed to be subcritical, indicating that the response will jump to another stable branch as the parameter moves past the bifurcation point. In practice (observed both physically and through numerical simulations), as one pushes the torque past this point 'N', the response typically jumps up onto the upper branch of the response curve.

It is important to note that the rotor response is generally favorable on the lower response branch, where the absorbers counteract the applied torque. In contrast, on the upper branch, the absorbers are in phase with the applied torque, thereby leading to increased torsional vibration levels of the rotor. To emphasize this, an additional dashed line is superimposed onto Figure 2 that represents the response with the absorbers locked in place at $s_i = 0$, their vertices. It should also be noted that in terms of design, one typically must live with a certain inertia ratio and damping level, but are free to set a desired level of mistuning of the absorbers by path selection. Generally, increasing the mistuning leads to an extended operating range, that is, the bifurcation points are pushed out to large torques, but performance is decreased over that range.

3. Experimental Component

Central to the experimental component of this work is the specially designed test apparatus. It is instrumented to accurately measure the applied torque, angular speed of the rotor, and the displacements of the absorbers. Moreover, it has a unique feature in that it allows one to continuously vary the order of the excitation, n . This is very convenient, since it is much easier to turn a dial than to reconfigure the hardware in order to vary the relative tuning between the

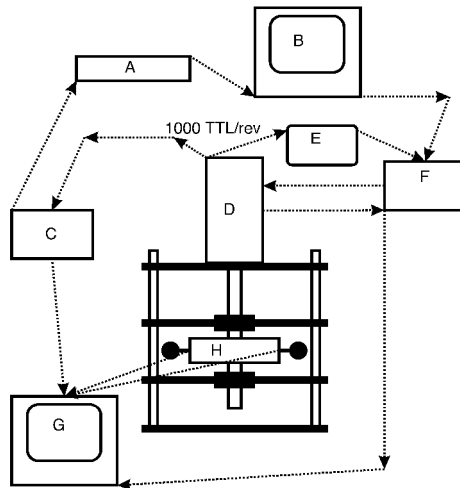


Figure 3. A schematic diagram of the experimental setup.

absorbers and the excitation. See, for example, Figure 9, which shows the response of the rotor acceleration as a function of the torque order, at a fixed torque amplitude. Note that such a frequency response curve is very valuable from the design point of view, but is not what occurs in a practical application where the order of the excitation is fixed. Here the response shows the desired tuning point, just to the left of the resonance.

A detailed description of the experimental apparatus can be found in [7] and only a brief outline is given in the next subsection. This is followed by a presentation of sample experimental results and a comparison with the theoretical predictions.

3.1. EXPERIMENTAL APPARATUS

A schematic of the experimental apparatus is shown in Figure 3. The main component is a servo motor (D) that drives a shaft with an attached flywheel (H). The shaft is securely constrained by two bearings, one above and one below the flywheel, and the complete assembly is surrounded by an aluminum frame. The absorbers are shown as two solid circles located at opposing sides of the flywheel.

The additional components serve as measuring or control devices. For example, the torque is controlled through a feedback system (F) that monitors the motor current. The command signal for this is obtained from two sources. One from the computer (B), which maintains the constant *mean* speed of the rotor, Ω , and the other from a signal generator (E) that supplies the desired fluctuating component of the torque. An important feature of the signal generator is that its time base is received *externally* from an encoder on the servo motor that produces 1,000 pulses/rev. Hence, if one wishes to impose a fluctuating torque that varied sinusoidally, say, 2 times per revolution then one programs the signal generator to increment through one complete sine wave for every 500 pulses it counts (in this case one would have $n = 2$). This feature allows torque fluctuations to be imposed that are any prescribed function of the *angular position* of the shaft. For example, although not reported in this document, it would be a simple matter to apply a torque that was exactly the same as an experimentally obtained torque variation obtained from a dynamometer test of a real engine. An additional feature of this set-up means that one can quite simply vary the order of the applied torque and hence

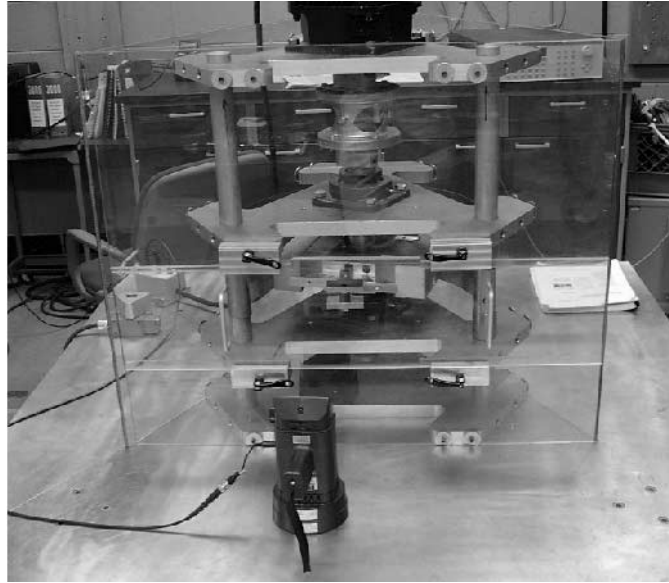


Figure 4. A general view of the experimental facility.

experimentally investigate the influence of mistuning between the absorber's tuning and the applied torque order. It should be emphasized again that this is not what typically occurs in a practical application, since in any particular design the order of the applied torque is fixed.

The remaining components indicated in Figure 3 are as follows. A frequency to voltage converter (C) is used to measure the instantaneous angular speed of the shaft. This signal can be further analyzed/recorded in the computer (G) and used to monitor the angular acceleration of the shaft (recall, this is the quantity one wishes to minimize by the correct design of the absorbers). The signal is also fed through a low pass filter (A) to monitor the mean angular speed of the shaft. A computer (B) closes a feedback loop that is designed to have a large time constant so it does not influence the higher frequency speed variations imposed by the applied fluctuating torque.

A picture of the physical system appears in Figure 4. This shows a general view of the aluminum structure that houses the shaft, flywheel and absorbers. Part of the servo motor that drives the system can be seen at the top of the picture. An additional sketch to show the design of the flywheel and the attached absorbers is shown in Figure 5. The peculiar shapes of the flywheel and the parts that hold the absorbers in place are to allow two additional absorbers to be attached at a later date. It will also accommodate a design for exploring the behavior of absorbers moving along noncircular paths. The location of the mini encoder that measures the angular position of the absorber is also indicated on this figure. Signals from this are carried out through the rotor using slip rings (not shown).

3.2. SYSTEM PARAMETER VALUES OF THE EXPERIMENT

Before being able to compare the experimental results to the theoretical predictions, one must obtain physical values for a number of the parameters of the system. This is done through a combination of direct measurements (e.g., length, mass) and a more involved set of tests, e.g., removing the absorbers and measuring the resulting angular acceleration of the rotor at different alternating torque levels. This latter test allows one to empirically obtain the inertia

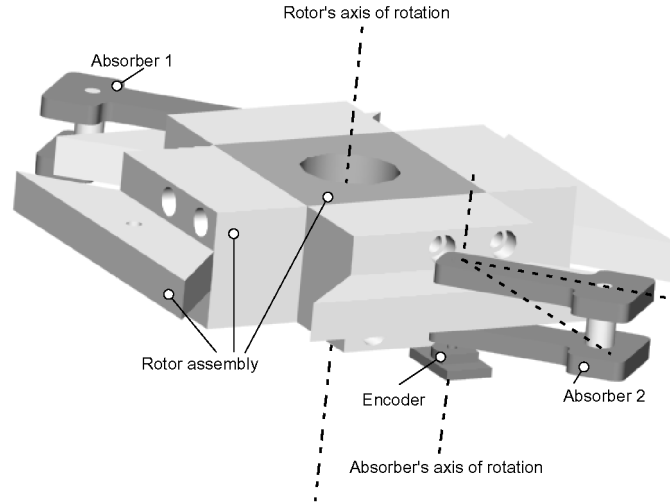


Figure 5. A schematic of the main flywheel (rotor) assembly with two pendulums attached.

of the rotor, J , through the relationship $T = J\ddot{\theta}$. It is difficult to evaluate the damping of the absorbers, μ_a , as they rotate and so a value is chosen that leads to a reasonable match in the measured response at resonance. This value is then used for all the results presented in this subsection.

The following is a list of the numerical quantities measured directly:

$$J = 0.1347 \text{ kg.m}^2$$

$$R_0 = 0.157 \text{ m}$$

$$R = 0.0118 \text{ m}$$

$$r = 0.039 \text{ m}$$

$$\rho = 0.0337 \text{ m}$$

$$m/2 = 0.282 \text{ kg (the individual mass of each of the two absorbers).}$$

The theoretically predicted absorber tuning \tilde{n} can now be calculated using Equation (4), which yields $\tilde{n} = 1.31$.

For the present absorber configuration, consisting of a compound pendulum, it is found that the inertia ratio is given by

$$\varepsilon = m(r^2 + \rho^2 + rR)^2 / (J(r^2 + \rho^2)) = mr^2(1 + \tilde{n}^2)/J, \quad (12)$$

which reduces to $\varepsilon = m(r + R)^2/J = mR_0^2/J$ for a point mass absorber, that is, with $\rho = 0$ (see [8] for details). Substituting the provided data into Equation (12) results in $\varepsilon = 0.0829$.

Finally, the mean speed of the rotor is set to $\Omega = 10\pi$ rad/s for all the experiments and the absorber damping is taken as $\tilde{\mu}_a = 0.126$, which this is equivalent to a damping ratio of 0.45% in the usual sense.

3.3. EXPERIMENTAL RESULTS

Figure 6 shows a combination of theoretical and experimental results for a case where the applied torque order, n , is held constant at 1.27, i.e., below the perfect linear absorber tuning level of $\tilde{n} = 1.31$. In addition, a dashed line is shown that represents the angular acceleration

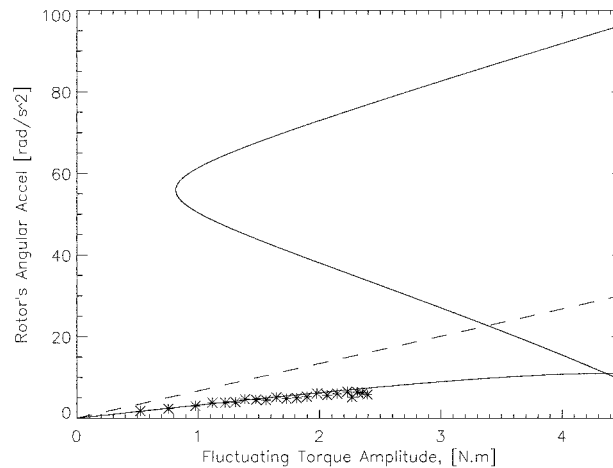


Figure 6. Comparison of the theoretical result (solid line) and the experimental data (*). Dashed line shows the response with the absorbers locked. $n = 1.27$.

of the flywheel, assuming the absorbers are locked in place (for clarity, no experimental data are plotted along this line, but they lie essentially right on top of it). Hence, any response below this dashed line indicates that using the absorbers will reduce the torsional vibration. At a torque level of approximately 2.4 N.m the system became unstable and a jump to a larger response occurs. Indeed, the response became so large after the jump occurred that no data could be collected as the motion of the absorbers were of the order of $\pm 90^\circ$. The physical design of the system caused them to hit against their supports and the test run had to be stopped. It should be noted that there is very good agreement between the theoretical and the experimental results before the system went unstable. This occurred well before the jump point (the theoretical saddle node bifurcation point is not shown on this figure, but occurs at a torque level of approximately 5 N.m). The reason for this is that the absorbers are losing stability due to the transition previously mentioned in Section 2.4 and shown as point 'N' in Figure 2.

This transition can be more clearly appreciated by viewing Figure 7. The torque order has now been increased to 1.29 and data was collected as the torque level was slowly increased (*) and then slowly decreased (+). For this value of n the lower branch of the theoretical curve has a horizontal tangency (which can be shown to be where the synchronous solution loses stability [1]) at a torque level of approximately 2.5 N.m. Admittedly this is still above the experimental value of 2.1 N.m, but it is harder to accurately predict a horizontal tangency than a vertical one. In this experimental run, data was collected as the torque was increased and then slowly decreased. One can clearly observe a hysteresis effect. While the torque level at which the jump down occurs is close to the theoretical prediction of 0.6 N.m, the amplitude agreement is not as close as it is on the lower branch. This is not surprising since if one calculates the associated absorbers' angular motion, it is found to be in the neighborhood of 70° , and it is unreasonable to expect the approximate solution technique employed to be able to accurately predict the behavior at such high levels. Of course, one could always seek more accurate approximate solutions by including additional terms, but it should be noted that the main aim of the analysis is to accurately predict the behavior of the rotor and the absorber while they are operating on the lower solution branches.

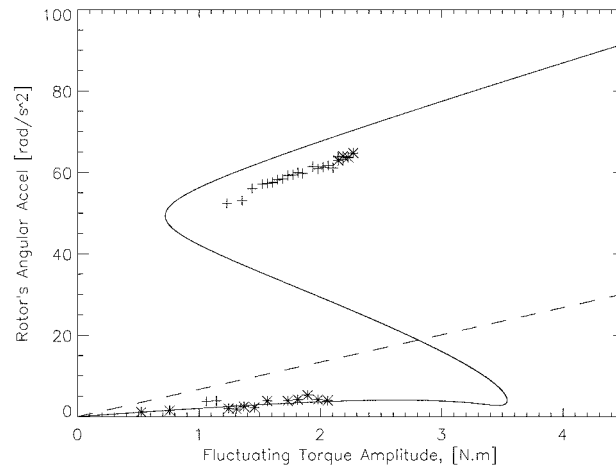


Figure 7. As in Figure 6, showing torque increasing (*) and decreasing (+) ($n = 1.29$).

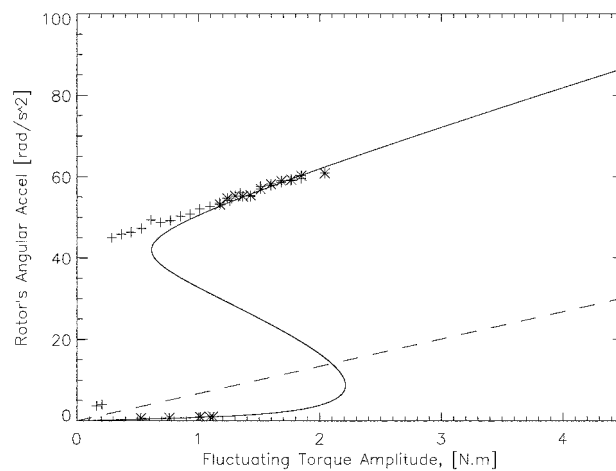


Figure 8. As in Figure 7, but with $n = 1.31$.

To complete this set of experiments, the torque order is increased to $n = 1.31$, i.e., perfectly in tune with the linear design \tilde{n} of the absorber. The results are shown in Figure 8. As predicted, acceleration of the rotor is smaller and the absorbers go unstable at a lower torque level. Hysteresis is again present. If n were increased even further, we would observe the right most saddle node continuing to move to lower torque levels. This is the reason that in practical designs one selects $\tilde{n} > n$, so that the system may operate over a larger torque range without going unstable. The disadvantage is that the absorbers are not so effective at reducing the angular acceleration of the rotor.

In addition to the previous three experiments, where the torque order was held constant and the level of the torque was varied, one can fix the level of the torque and vary the order (i.e., the frequency) of the applied torque. As previously stated, this is *not* what happens in practice. By running such tests, we can study how robust particular designs are, e.g., how close to instabilities particular operating regimes are. To this end, experiments were run for torque levels of 0.5, 1.5, and 3.0 N.m. The results are shown in Figures 9, 10, and 11, respectively. It should be stressed that in these plots, the rotor's angular acceleration is normalized by the

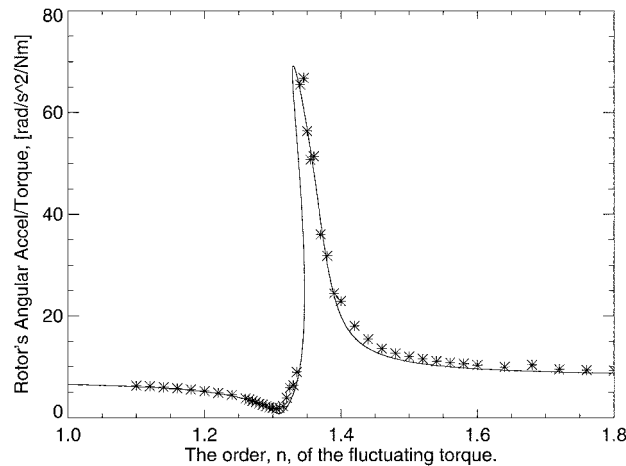


Figure 9. Comparison of the theoretical result (solid line) and the experimental data (*). Alternating torque = 0.5 N.m.

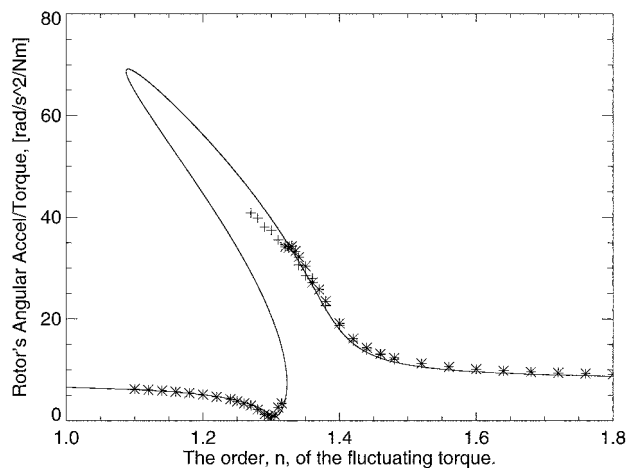


Figure 10. Comparison of the theoretical result (solid line) and the experimental data (* is for n increasing, + is for n decreasing). Alternating torque = 1.5 N.m.

amplitude of the applied torque, thus allowing one to better compare all three plots. In the three figures the minimum rotor acceleration point is clearly defined. It is always close to the value of 1.31. Less clear (but observable) is its shift to slightly lower values as the level of the torque, and hence the amplitude of the absorbers, is increased. This is due to the softening nonlinear effect of the absorbers moving on a circular path. More important is the fact that when the torque level is 3.0 N.m (Figure 11) the minimum point cannot be reached, as the response on the lower branch is experimentally found to be unstable at the turning point. Indeed, if the torque order is slowly increased (data points *) from a low level, an instability occurs at approximately $n = 1.26$ and the experiment has to be aborted due to the absorbers hitting their maximum displacement limits. If the experiment is restarted at a high level of n and then n is reduced (data points +), it is possible to move along the top branch until approximately $n = 1.26$ and then the absorbers once again reach their displacement limit. Of course, this is a practical limit imposed by the design, whereas the mathematical solution

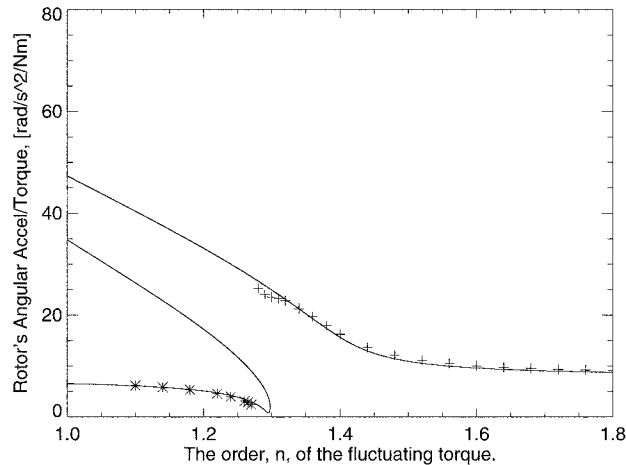


Figure 11. Comparison of the theoretical result (solid line) and the experimental data (* is for n increasing, + is for n decreasing). Alternating torque = 3.0 N.m.

has no such restriction, at least to the level of accuracy employed. Hence the reason for the theoretical solution continuing to exist at extremely high levels.

4. Concluding Remarks

The experimental results have shown how the angular acceleration of a rotor acted on by an alternating torque can be influenced by the addition of pendulum absorbers. The results clearly show regions in the parameter space where the absorbers effectively reduce the torsional vibration of the rotor, and other regions where the absorbers lose stability, with a net result of more severe vibration. In general, the theoretical and experimental results are in good agreement. One reason for some of the discrepancies is that a first order approximate solution has been sought, this only being accurately for small to medium absorber displacements. Another point to note is that the theoretical results presented herein assume that the absorbers all have the same physical parameters, i.e., damping and tuning. Work is underway to experimentally quantify differences that may be present and to intentionally introduce such variations.

Other planned extensions to the work are to experimentally investigate noncircular absorber paths, vary the spin rate Ω as a function of time (i.e., spin-up and spin-down experiments), and to change the form of the applied fluctuating torque.

Acknowledgements

This work was supported by NSF under grants number CMS-9700143 and CMS-0084947. The authors also wish to acknowledge help provided by the following students: Reimund Keiser, Yi Wu, Mark Berry and Tyler Nester.

References

1. Alsuwaiyan, A. H. and Shaw, S. W., 'Performance and dynamic stability of general-path centrifugal pendulum vibration absorbers', *Journal of Sound and Vibration* **252**, 2002, 791–815.
2. Albright, M., Crawford, T., and Speckart, F., 'Dynamic testing and evaluation of the torsional vibration absorber', SAE Paper No. 942519, 1994.
3. Denman, H. H., 'Tautochronic bifilar pendulum torsional absorbers for reciprocating engines', *Journal of Sound and Vibration* **159**, 1992, 251–277.
4. Newland, D. E., 'Nonlinear aspects of the performance of centrifugal pendulum vibration absorbers', *ASME Journal of Engineering for Industry* **86**, 1964, 257–263.
5. Chao, C. P., Lee, C. T., and Shaw, S. W., 'Stability of the unison response for a rotating system with multiple tautochronic pendulum vibration absorbers', *ASME Journal of Applied Mechanics* **64**, 1996, 149–156.
6. Chao, C. P., Lee, C. T., and Shaw, S. W., 'Non-unison dynamics of multiple centrifugal pendulum vibration absorbers', *Journal of Sound and Vibration* **64**, 1997, 769–794.
7. Haddow, A. G. and Shaw, S. W., 'Torsional vibration absorbers: A testing and evaluation apparatus', in *Proceedings of the SAE Noise and Vibration Conference*, 2001, Paper No. 01NVC1577.
8. Nester, T. M., 'Experimental investigation of circular path centrifugal pendulum vibration absorbers', Master's Thesis, Michigan State University, City, MI, 2002.